International Journal of Structural Stability and Dynamics
Vol. 10, No. 3 (2010) 529–554

DOI: 10.1142/S0219455410003609

World Scientific
www.worldscientific.com

BRIDGE VIBRATION UNDER VEHICULAR LOADS: TIRE PATCH CONTACT VERSUS POINT CONTACT

XINFENG YIN[*,†], C. S. CAI[†,‡,§], ZHI FANG[*] and LU DENG[†]

[*]*College of Civil Engineering, Hunan University*
Changsha China 410082

[†]*Department of Civil and Environmental Engineering*
Louisiana State University, Baton Rouge
Louisiana 70803, USA

[‡]*School of Civil Engineering and Architecture*
Changsha University of Science and Technology
45 Chiling Road, Tianxin Distr. 410076
Changsha, Hunan, China
[§]*CSCAI@LSU.EDU*

Received 29 July 2009
Accepted 16 September 2009

When establishing the equations of motion of the bridge-vehicle coupling system, most researchers simplify the contact between the vehicle tire and road surface as a point contact. In reality, a vehicle tire deforms and makes contact with the road surface over a footprint area called patch contact. This paper presents a new method that allows for the effect of the patch contact on the dynamic response of the bridge-vehicle coupling system. In this method, the vehicle tire is modeled as a two-dimensional elementary spring model, and the patch contact is assumed to be a rectangle. The bridge-vehicle coupling equations are established by combining the equations of motion of both the bridge and vehicle using the displacement relationship and interaction force relationship at the patch contact. A series of simulation studies have been carried out in which the effects of various factors such as vehicle speed, tire stiffness and damping, size of the patch contact, number of vehicles, and faulting condition have been investigated. The numerical simulations and field test results show that the proposed method can more rationally simulate the interaction between the bridge and vehicles.

Keywords: Bridge-vehicle coupling system; bridge; vehicle; vibration; tire; patch contact; point contact.

1. Introduction

The interaction between a bridge and vehicles has attracted much attention over the last two decades due to a significant increase of heavy and high-speed vehicles in highway and railway traffic. By modeling a moving vehicle as a moving load, moving

[§]Corresponding author.

mass or moving sprung mass, the dynamic response of bridges induced by moving vehicles has been studied by many researchers.[1−3] Some complicated vehicle models that can consider the various dynamic properties of vehicles have been introduced for the bridge-vehicle interactions.[4−6]

According to Yang *et al.*,[7] there are two approaches for solving the bridge-vehicle interaction problems. One approach is to divide the bridge-vehicle system into two subsystems with an interface between the bridge and vehicle. Two sets of equations of motion can be written, one for the supporting bridge and the other for each of the moving vehicles. In order to solve the two sets of differential equations, procedures of interactive nature are often adopted, though the equations can be solved simultaneously without iteration.[8,9] In this case, one may first start by assuming the displacement for the contact points, and then solve the vehicle equations to obtain the contact forces. By substituting the contact forces into the bridge equations, improved displacements at the contact points can be obtained. It is the interaction or contact forces existing at the contact points of the two subsystems that make the two sets of equations coupled. These single contact points are used to model the relationship of a vehicle tire and road surface in most studies.[10−14] The other approach for solving the vehicle-bridge interaction problems includes those based on the condensation method, which focuses on formulating a bridge-vehicle interaction element. First, two sets of equations of motion need to be written, one for the bridge element and the other for the sprung mass lumped from the vehicle directly acting on the element. The sprung mass equations are discretized using finite difference formulas, and condensed to those of the bridge element by the contact points, which will result in the so-called bridge-vehicle interaction element. The condensation approach also assumes the interface between a vehicle tire and the road surface as a single point contact.[15−18]

While it may be reasonable to simulate the interfaces between the wheels and road surface as point contacts for trains with steel wheelsets, it is not the case for vehicles moving on the highway bridges. This is because their tires deform and make contact with the road surface over a footprint area called patch contact. While the effect of different contact models between the tire and road surface, point contact or patch contact, on the vibration of vehicles has been studied by many researchers,[19−23] hitherto no studies have been made for the effect of the contact condition on bridge vibrations.

This paper presents a new method that allows for the effect of the patch contact on the dynamic response of the bridge-vehicle coupling system. This method mainly focuses on establishing a new tire model, which is a two-dimensional elementary spring model, to study the effect of the patch contact on the dynamic response of the bridge-vehicle coupling system. The patch contact between the tires and road surface is assumed to be a rectangle. The displacement relationship and the interaction force relationship at the patch contact are used to establish the equations of motion of the bridge-vehicle coupling system. A series of simulation studies have been carried out with the view to examine the effects of various factors such as vehicle speed, tire

stiffness and damping, size of the contact patch, number of vehicles, and faulting condition. The numerical simulations and field measurements show that the proposed method can more rationally simulate the interaction of the bridge-vehicle coupling system.

2. Bridge-Vehicle Coupled System

2.1. *Vehicle model*

A review of vehicle models was made by Yu and Chan.[24] As discussed earlier, in reality the tire and road surface is not in contact at a point, but rather in the form of a patch. In this study, a new full-scale vehicle model with seven degree-of-freedoms (DOFs) is used as shown in Fig. 1. These DOFs are the vertical displacement of truck body (y_t), pitching rotation of truck body (θ_t), vertical displacement of truck front axle (y_a^1), vertical displacement of truck rear axle (y_a^2), roll displacement of truck body (ϕ_t), roll displacement of truck front axle (ϕ_a^1), and roll displacement of truck rear axle (ϕ_a^2). To simulate the interaction between the vehicle tire and road surface, the tire is modeled as a two-dimensional elementary spring model shown in Fig. 2, and the mass of the tire can be neglected since it is small when compared to the total mass of the vehicle.

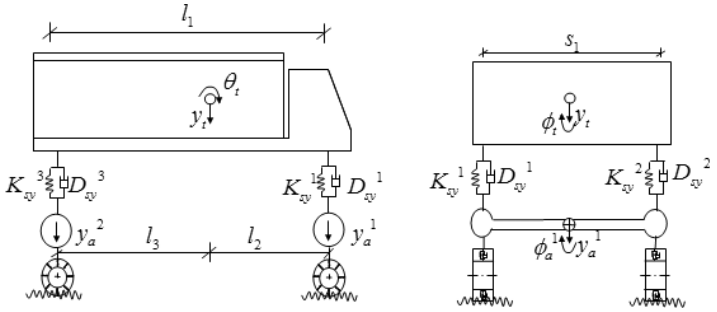

Fig. 1. A full-scale vehicle model.

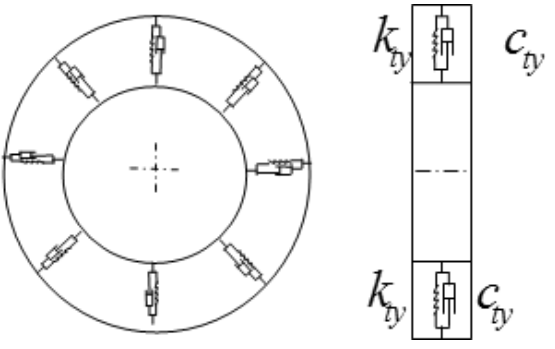

Fig. 2. A tire model.

The relative displacements of the suspension springs can be written as:

$$U_{sy}^{1} = (y_t - y_a^1) + (s_1/2)(\phi_t - \phi_a^1) + l_2\theta_t, \tag{1}$$

$$U_{sy}^{2} = (y_t - y_a^1) - (s_1/2)(\phi_t - \phi_a^1) + l_2\theta_t, \tag{2}$$

$$U_{sy}^{3} = (y_t - y_a^2) + (s_2/2)(\phi_t - \phi_a^2) - l_3\theta_t, \tag{3}$$

$$U_{sy}^{4} = (y_t - y_a^2) - (s_2/2)(\phi_t - \phi_a^2) - l_3\theta_t, \tag{4}$$

where s_1 is the distance between the right and left tires of the front axle; s_2 the distance between the right and left tires of the rear axle; l_2 the distance between the front axle and the gravity center of the vehicle body; and l_3 the distance between the rear axle and the gravity center of the vehicle body.

The elastic and damping forces of the suspension can be written as:

$$F_{sy}^{i} = K_{sy}^{i} U_{sy}^{i}, \tag{5}$$

$$F_{dsy}^{i} = D_{sy}^{i} \dot{U}_{sy}^{i}, i = 1, 2, 3, 4, \tag{6}$$

where K_{sy}^{i} is the suspension spring stiffness of the ith axle; and D_{sy}^{i} the suspension damper coefficient of the ith axle.

The displacement in the radial direction of the ith tire spring (see Fig. 3) at the contact position x can be expressed as:

$$U_{tyx}^{1} = \{y_a^1 + (s_1/2)\phi_a^1 - [-r(x)^1] + \Delta^1 - R(1 - \cos\ \theta) - y_{bx\_contact}^{1}\}/\cos\ \theta, \tag{7}$$

$$U_{tyx}^{2} = \{y_a^1 - (s_1/2)\phi_a^1 - [-r(x)^2] + \Delta^2 - R(1 - \cos\ \theta) - y_{bx\_contact}^{2}\}/\cos\ \theta, \tag{8}$$

$$U_{tyx}^{3} = \{y_a^2 + (s_2/2)\phi_a^2 - [-r(x)^3] + \Delta^3 - R(1 - \cos\ \theta) - y_{bx\_contact}^{3}\}/\cos\ \theta, \tag{9}$$

$$U_{tyx}^{4} = \{y_a^2 - (s_2/2)\phi_a^2 - [-r(x)^4] + \Delta^4 - R(1 - \cos\ \theta) - y_{bx\_contact}^{4}\}/\cos\ \theta, \tag{10}$$

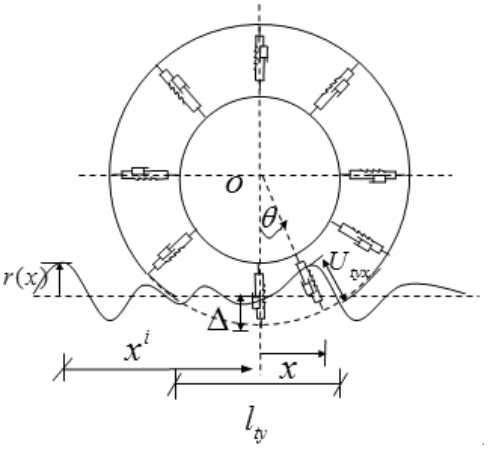

Fig. 3. Tire deformation model.

where

$$\cos\ \theta = \frac{R - \Delta^{i=1,2,3,4}}{\sqrt{(x)^2 + (R - \Delta^{i=1,2,3,4})^2}}.$$

From Eqs. (7) to (10), one can observe that $U^i_{tyx} i = 1, 2, 3, 4$ is a function of the truck axle displacement $y^i_a i = 1, 2$; roll displacement of truck axle $\phi^i_a i = 1, 2$; road roughness $r(x)^i i = 1, 2, 3, 4$; tire radius R; the tire deformation due to the load of vehicle weight $\Delta^i i = 1, 2, 3, 4$; and the bridge dynamic deflection at the contact position $xy^i_{bx\_contact} i = 1, 2, 3, 4$.

In the following equations, "F" stands for "force", subscription "ty" for "tire", "dty" for "damping of tire", "sy" for "suspension", and "dsy" for "damping of suspension". Therefore, the interaction forces acting on the bridge through the patch length l_{ty} of the ith tire can be written as:

$$F^i_{ty} = \int_{x^i - l_{ty}/2}^{x^i + l_{ty}/2} k^i_{ty} U^i_{tyx}\ \cos\ \theta dx, \tag{11}$$

$$F^i_{dty} = \int_{x^i - l_{ty}/2}^{x^i + l_{ty}/2} c^i_{ty} \dot{U}^i_{tyx}\ \cos\ \theta dx, \tag{12}$$

where k^i_{ty} and c^i_{ty} are the radial direction spring stiffness and damper coefficients of the ith tire, respectively; and x^i is the position of the ith tire patch center.

The equations of motion of the vehicle can be obtained from the Lagrangian formulation, and can be written as:

$$m_t \ddot{y}_t + (F^1_{sy} + F^2_{sy} + F^3_{sy} + F^4_{sy}) + (F^1_{dsy} + F^2_{dsy} + F^3_{dsy} + F^4_{dsy}) = m_t g, \tag{13}$$

$$\begin{aligned} I_{xt}\, \ddot{\phi}_t + (s_1/2)(F^1_{sy} - F^2_{sy}) + (s_2/2)(F^3_{sy} - F^4_{sy}) \\ +\ (s_1/2)(F^1_{dsy} - F^2_{dsy}) + (s_2/2)(F^3_{dsy} - F^4_{dsy}) = 0, \end{aligned} \tag{14}$$

$$I_{zt}\ddot{\theta}_t + l_2(F^1_{sy} + F^2_{sy}) - l_3(F^3_{sy} + F^4_{sy}) + l_2(F^1_{dsy} + F^2_{dsy}) - l_3(F^3_{dsy} + F^4_{dsy}) = 0, \tag{15}$$

$$m_{a1}\ddot{y}^1_a - (F^1_{sy} + F^2_{sy}) + (F^1_{ty} + F^2_{ty}) - (F^1_{dsy} + F^2_{dsy}) + (F^1_{dty} + F^2_{dty}) = m_{a1} g, \tag{16}$$

$$\begin{aligned} I_{xa1}\, \ddot{\phi}^1_a - (s_1/2)(F^1_{sy} - F^2_{sy}) + (s_1/2)(F^1_{ty} - F^2_{ty}) \\ -\ (s_1/2)(F^1_{dsy} - F^2_{dsy}) + (s_1/2)(F^1_{dty} - F^2_{dty}) = 0, \end{aligned} \tag{17}$$

$$m_{a2}\ddot{y}^2_a - (F^3_{sy} + F^4_{sy}) + (F^3_{ty} + F^4_{ty}) - (F^3_{dsy} + F^4_{dsy}) + (F^3_{dty} + F^4_{dty}) = m_{a2} g, \tag{18}$$

$$\begin{aligned} I_{xa2}\, \ddot{\phi}^2_a - (s_2/2)(F^3_{sy} - F^4_{sy}) + (s_2/2)(F^3_{ty} - F^4_{ty}) \\ -\ (s_2/2)(F^3_{dsy} - F^4_{dsy}) + (s_2/2)(F^3_{dty} - F^4_{dty}) = 0, \end{aligned} \tag{19}$$

where m_t is the mass of truck body; I_{xt} and I_{zt} are the rolling and pitching moment of inertia of truck body, respectively; m_{a1} and m_{a2} are the mass of the front and rear axles, respectively; and I_{xa1} and I_{xa2} are rolling moment of inertia of the front and rear axles, respectively.

Equations (13)−(19) can be rewritten in a matrix form as:

$$[M_v]\{\ddot{y}_v\} + [C_v]\{\dot{y}_v\} + [K_v]\{y_v\} = \{F_G\} + \{F_{v-b}\}, \tag{20}$$

where $[M_v]$, $[C_v]$, and $[K_v]$ = the mass, damping, and stiffness matrices of the vehicle, respectively; $\{y_v\}$ = the displacement vector of the vehicle; $\{F_G\}$ = gravity force vector of the vehicle; and $\{F_{v-b}\}$ = vector of the wheel-road contact forces acting on the vehicle.

2.2. *Bridge model*

The equation of motion of a bridge can be written as:

$$[M_b]\{\ddot{y}_b\} + [C_b]\{\dot{y}_b\} + [K_b]\{y_b\} = \{F_{b-v}\}, \tag{21}$$

where $[M_b]$, $[C_b]$, and $[K_b]$ are the mass, damping, and stiffness matrices of the bridge, respectively; $\{y_b\}$ is the displacement vector for all DOFs of the bridge; $\{\dot{y}_b\}$ and $\{\ddot{y}_b\}$ are the first and second derivative of $\{y_b\}$ with respect to time, respectively; and $\{F_{b-v}\}$ is a vector containing all external forces acting on the bridge.

2.3. *Assembling the vehicle-bridge coupled system*

Vehicles traveling on a bridge are connected to the bridge via patch contacts. The interaction forces acting on the bridge $\{F_{b-v}\}$ and the interaction forces acting on the vehicles $\{F_{v-b}\}$ are actually action and reaction forces existing at the patch contact. In terms of finite element modeling, these interaction forces may not be applied right at any node. Therefore, the interaction forces need to be transformed into equivalent nodal forces $\{F_b^{eq}\}$ in the finite element analysis. This can be done using the virtual work principle, which states that the work done by the equivalent nodal forces and the actual force should be equal, which can be expressed as:

$$\{y_{b\_nodal}\}^T\{F^{eq}\} = y_{bx\_contact} \cdot F, \tag{22}$$

where $\{y_{b\_nodal}\}$ is the displacement vector for all the nodes of the element in contact; $y_{bx\_contact}$, the displacement of the element bearing the tire spring load at the contact position x; $\{F^{eq}\}$ the equivalent force vector applied at all the nodes of the element in contact; and F the real force acting at the patch contact.

The $y_{bx\_contact}$ can be expressed using the displacement at each node of the element as:

$$y_{bx\_contact} = [N_e]\{y_{b\_nodal}\}, \tag{23}$$

where $[N_e]$ is the relationship function of the element in contact. In view of Eqs. (22) and (23), we can easily obtain the following relationship between the equivalent nodal forces and the interaction force acting on the element in contact:

$$\{F^{eq}\} = [N_e]^T \cdot F. \tag{24}$$

To be consistent with the size of the force vector $\{F_b^{eq}\}$ in the analysis of the full bridge, Eq. (24) can be expanded to a full force vector form as:

$$\{F_b^{eq}\} = [N_b]^T \cdot F, \tag{25}$$

where $\{F_b^{eq}\}$ is a vector with the number of elements equal to the total number of DOFs of the bridge. It is constructed by inserting the elements in the original force vector $\{F^{eq}\}$ in Eq. (24) into their corresponding DOFs in the full force vector $\{F_b^{eq}\}$ and adding zero terms to the remaining elements in $\{F_b^{eq}\}$. For two interaction forces acting upon different elements of the same bridge, the relationship function of the bridge $[N_b]$ for the two forces would be different though the element relationship function $[N_e]$ may be the same, because the corresponding DOFs of the non-zero terms in the two force vectors are different.

In a bridge-vehicle system, the relationship among the vertical displacement of vehicle body y_v^i, bridge deflection at the contact position $y_{bx\_contact}^i$, the radial deformation of ith tire spring U_{tyx}^i at the position x, and road surface profile $r(x)^i$, shown in Eqs. (7)−(10), can be rewritten as:

$$\begin{aligned} U_{tyx}^i &= \{y_v^i - [-r(x)^i] - y_{bx\_contact}^i\}/\cos\ \theta \\ y_v^i &= y_a^j \pm (s_j/2)\phi_a^j + \Delta^i\_R(1-\cos\ \theta), \quad j = 1, 2. \end{aligned} \tag{26}$$

The first derivative of Eq. (26) can then be obtained as:

$$\dot{U}_{tyx}^i = (\dot{y}_v^i + (x)^i - \dot{y}_{bx\_contact}^i)/\cos\ \theta, \tag{27}$$

where $\dot{y}_v^i$ is the velocity of the vehicle body in the vertical direction; $\dot{r}(x)^i = \frac{dr(x)^i}{dx}\frac{dx}{dt} = \frac{dr(x)^i}{dx}v(t)$, where $v(t)$ is the vehicle traveling velocity; and $y_{bx\_contact}^i$, according to the definition of the relationship function of the bridge in Eq. (23), can be expressed as:

$$y_{bx\_contact}^i = [N_e] \cdot \{y_{b\_nodal}^i\} = [N_b] \cdot \{y_b\}. \tag{28}$$

The interaction force acting on the ith tire can be obtained as:

$$\begin{aligned} F_{v-b}^i &= -F_{ty}^i - F_{dty}^i \\ &= -\int_{x^i - l_{ty}/2}^{x^i + l_{ty}/2} k_{ty}^i (y_v^i + r(x)^i - [N_b^i]\{y_b\})dx \\ &\quad - \int_{x^i - l_{ty}/2}^{x^i + l_{ty}/2} c_{ty}^i \left(\dot{y}_v^i - \frac{d[N_b^i]}{dx} v^i(t)\{y_b\} - [N_b^i]\{\dot{y}_b\} + \frac{dr(x)^i}{dx} v^i(t) \right) dx. \end{aligned} \tag{29}$$

Comparing the length of l_{ty} with the total length of the bridge, l_{ty} can be regarded as small. Therefore, the value of y_b and y_v can be assumed to be a constant in the length

range form $x^i - l_{ty}/2$ to $x^i + l_{ty}/2$. Equation (29) can be further written as:

$$\begin{aligned} F^i_{v-b} &= -\int_{x^i-l_{ty}/2}^{x^i+l_{ty}/2} k^i_{ty}(y^i_v + r(x)^i - [N^i_b]\{y_b\})dx \\ &\quad -\int_{x^i-l_{ty}/2}^{x^i+l_{ty}/2} c^i_{ty}\left(\dot{y}^{\,i}_v - \frac{d[N^i_b]}{dx}v^i(x)\{y_b\} - [N^i_b]\{\dot{y}_b\} + \frac{dr(x)^i}{dx}v^i(t)\right)dx \\ &= -\int_{x^i-l_{ty}/2}^{x^i+l_{ty}/2} k^i_{ty}dxy^i_v - \int_{x^i-l_{ty}/2}^{x^i+l_{ty}/2} k^i_{ty}r(x)^i dx + \int_{x^i-l_{ty}/2}^{x^i+l_{ty}/2} k^i_{ty}[N^i_b]dx\{y_b\} \\ &\quad -\int_{x^i-l_{ty}/2}^{x^i+l_{ty}/2} c^i_{ty}dx\dot{y}^{\,i}_v + \int_{x^i-l_{ty}/2}^{x^i+l_{ty}/2} c^i_{ty}\frac{d[N^i_b]}{dx}v^i(t)dx\{y_b\}, \\ &\quad +\int_{x^i-l_{ty}/2}^{x^i+l_{ty}/2} c^i_{ty}[N^i_b]dx\{\dot{y}_b\} - \int_{x^i-l_{ty}/2}^{x^i+l_{ty}/2} c^i_{ty}\frac{dr(x)^i}{dx}v^i(t)dx, \end{aligned} \tag{30}$$

where $[N^i_b]$ is the relationship function of the bridge for an interaction force between the ith tire and the bridge.

The N interaction forces can be expressed in a vector form as:

$$\begin{aligned} \{F^N_{v-b}\} &= \{F^1_{v-b} \quad F^2_{v-b}\cdots F^N_{v-b}\}^T \\ &= -[K^N_{v-v}]\{y_v\} - \{F_{v-r}\} + [K_{v-b}]\{y_b\} - [C^N_{v-v}]\{\dot{y}_v\} \\ &\quad + [K_{v-cb}]\{y_b\} + [C_{v-b}]\{\dot{y}_b\} - \{F_{v-cr}\}, \end{aligned} \tag{31}$$

where $[K^N_{v-v}]$ and $[C^N_{v-v}]$ are the stiffness, and damping matrices for N tires, respectively; and $[K_{v-b}]$, $\{F_{v-r}\}$, $[K_{v-cb}]$, $[C_{v-b}]$, and $\{F_{v-cr}\}$ are defined, respectively, as:

$$[K^N_{v-v}] = \left[\int_{x^1-l_{ty}/2}^{x^1+l_{ty}/2} k^1_{ty}dx \int_{x^2-l_{ty}/2}^{x^2+l_{ty}/2} k^2_{ty}dx \cdots \int_{x^N-l_{ty}/2}^{x^N+l_{ty}/2} k^N_{ty}dx\right];$$

$$[C^N_{v-v}] = \left[\int_{x^1-l_{ty}/2}^{x^1+l_{ty}/2} c^1_{ty}dx \int_{x^2-l_{ty}/2}^{x^2+l_{ty}/2} c^2_{ty}dx \cdots \int_{x^N-l_{ty}/2}^{x^N+l_{ty}/2} c^N_{ty}dx\right];$$

$$\begin{aligned} [K_{v-b}] &= [K^N_{v-v}] \\ &\quad \cdot \left[\int_{x^1-l_{ty}/2}^{x^1+l_{ty}/2} [N^1_b]^T dx \int_{x^2-l_{ty}/2}^{x^2+l_{ty}/2} [N^2_b]^T dx \cdots \int_{x^N-l_{ty}/2}^{x^N+l_{ty}/2} [N^N_b]^T dx\right]^T; \end{aligned}$$

$$\begin{aligned} \{F_{v-r}\} &= [K^N_{v-v}] \\ &\quad \cdot \left[\int_{x^1-l_{ty}/2}^{x^1+l_{ty}/2} r(x)^1 dx \int_{x^2-l_{ty}/2}^{x^2+l_{ty}/2} r(x)^2 dx \cdots \int_{x^N-l_{ty}/2}^{x^N+l_{ty}/2} r(x)^N dx\right]^T; \end{aligned}$$

$$[K_{v-cb}] = [C_{v-v}^{N}]\left[\int_{x^1-l_{ty}/2}^{x^1+l_{ty}/2} \frac{d[N_b^1]^T}{dx} v^1(t)dx \times \int_{x^2-l_{ty}/2}^{x^2+l_{ty}/2} \frac{d[N_b^2]^T}{dx} v^2(t)dx \cdots \int_{x^N-l_{ty}/2}^{x^N+l_{ty}/2} \frac{d[N_b^N]^T}{dx} v^N(t)dx\right]^T;$$

$$[C_{v-b}] = [C_{v-v}^{N}] \cdot \left[\int_{x^1-l_{ty}/2}^{x^1+l_{ty}/2} [N_b^1]^T dx \int_{x^2-l_{ty}/2}^{x^2+l_{ty}/2} [N_b^2]^T dx \cdots \int_{x^N-l_{ty}/2}^{x^N+l_{ty}/2} [N_b^N]^T dx\right]^T;$$

$$\{F_{v-cr}\} = [C_{v-v}^{N}] \cdot \left[\int_{x^1-l_{ty}/2}^{x^1+l_{ty}/2} \frac{dr(x)^1}{dx} v^1(t)dx \times \int_{x^2-l_{ty}/2}^{x^2+l_{ty}/2} \frac{dr(x)^2}{dx} v^2(t)dx \cdots \int_{x^N-l_{ty}/2}^{x^N+l_{ty}/2} \frac{dr(x)^N}{dx} v^N(t)dx\right]^T$$

As discussed earlier, the interaction forces acting on the bridge, $\{F_{b-v}\}$, are the reaction forces of that acting on the vehicles, $\{F_{v-b}\}$. Therefore, the following relationship holds:

$$\{F_{b-v}\} = -\{F_{v-b}\}. \tag{32}$$

By substituting Eqs. (30) and (32) into Eq. (25), the transformed equivalent nodal forces due to the N interaction forces are given by

$$\begin{aligned}\{F_b^{eq}\} &= \sum_{i=1}^{N} [N_b^i]^T \cdot (-F_{v-b}^i) \\ &= \sum_{i=1}^{N} [N_b^i]^T \cdot \left[\begin{array}{l} \displaystyle\int_{x^i-l_{ty}/2}^{x^i+l_{ty}/2} k_{ty}^i dx y_v^i + \int_{x^i-l_{ty}/2}^{x^i+l_{ty}/2} k_{ty}^i r(x)^i dx \\ \quad \displaystyle - \int_{x^i-l_{ty}/2}^{x^i+l_{ty}/2} k_{ty}^i [N_b^i] dx \{y_b\} + \int_{x^i-l_{ty}/2}^{x^i+l_{ty}/2} c_{ty}^i dx \dot{y}_v^i \\ \quad \displaystyle - \int_{x^i-l_{ty}/2}^{x^i+l_{ty}/2} c_{ty}^i \frac{d[N_b^i]}{dx} v^i(t)dx \{y_b\} \\ \quad \displaystyle - \int_{x^i-l_{ty}/2}^{x^i+l_{ty}/2} c_{ty}^i [N_b^i] dx \{\dot{y}_b\} + \int_{x^i-l_{ty}/2}^{x^i+l_{ty}/2} c_{ty}^i \frac{dr(x)^i}{dx} v^i(t)dx \end{array}\right], \\ &= [K_{b-v}]\{y_v\} + \{F_{b-r}\} - [K_{b-vb}]\{y_b\} + [C_{b-v}]\{\dot{y}_v\} \\ &\quad - [K_{b-cb}]\{y_b\} - [C_{b-b}]\{\dot{y}_b\} + \{F_{b-cr}\}\end{aligned} \tag{33}$$

where $[K_{b-v}]$, $[K_{b-vb}]$, $\{F_{b-r}\}$, $[C_{b-v}]$, $[K_{b-cb}]$, $[C_{b-b}]$, and $\{F_{b-cr}\}$ are defined as:

$$[K_{b-v}] = \left\{ [N_b^1]^T \cdot \int_{x^1-l_{ty}/2}^{x^1+l_{ty}/2} k_{ty}^1 dx [N_b^2]^T \cdot \int_{x^2-l_{ty}/2}^{x^2+l_{ty}/2} k_{ty}^2 dx \cdots [N_b^N]^T \cdot \int_{x^N-l_{ty}/2}^{x^N+l_{ty}/2} k_{ty}^N dx \right\};$$

$$[K_{b-vb}] = \sum_{i=1}^{n} [N_b^i]^T \int_{x^i-l_{ty}/2}^{x^i+l_{ty}/2} k_{ty}^i [N_b^i] dx;$$

$$\{F_{b-r}\} = \sum_{i=1}^{n} [N_b^i]^T \int_{x^i-l_{ty}/2}^{x^i+l_{ty}/2} k_{ty}^i r(x)^i dx;$$

$$[C_{b-v}] = \left\{ [N_b^1]^T \int_{x^1-l_{ty}/2}^{x^1+l_{ty}/2} c_{ty}^1 dx [N_b^2]^T \int_{x^2-l_{ty}/2}^{x^2+l_{ty}/2} c_{ty}^2 dx \cdots [N_b^N]^T \int_{x^N-l_{ty}/2}^{x^N+l_{ty}/2} k_{ty}^N dx \right\};$$

$$[K_{b-cb}] = \sum_{i=1}^{n} [N_b^i]^T \int_{x^i-l_{ty}/2}^{x^i+l_{ty}/2} c_{ty}^i \frac{d[N_b^i]}{dx} v^i(t) dx;$$

$$[C_{b-b}] = \sum_{i=1}^{n} [N_b^i]^T \int_{x^i-l_{ty}/2}^{x^i+l_{ty}/2} c_{ty}^i [N_b^i] dx;$$

$$\{F_{b-cr}\} = \sum_{i=1}^{n} [N_b^i]^T \int_{x^i-l_{ty}/2}^{x^i+l_{ty}/2} c_{ty}^i \frac{dr(x)^i}{dx} v^i(t) dx;$$

By substituting Eq. (31) into Eq. (20), we have:

$$\begin{aligned} &[M_v^N]\{\ddot{y}_v\} + [C_v^N]\{\dot{y}_v\} + [K_v^N]\{y_v\} \\ &\quad = F_G^N - [K_{v-v}^N]\{y_v\} + [K_{v-b}]\{y_b\} - \{F_{v-r}\} - [C_{v-v}^N]\{\dot{y}_v\} \\ &\quad + [K_{v-cb}]\{y_b\} + [C_{v-b}]\{\dot{y}_b\} - \{F_{v-cr}\}. \end{aligned} \tag{34}$$

Since $\{F_b^{eq}\}$ in Eq. (33) is actually the equivalent force vector of the external force vector $\{F_{b-v}\}$ in Eq. (21), after substituting Eq. (21) into Eq. (21), the following can be obtained:

$$\begin{aligned} &[M_b]\{\ddot{y}_b\} + [C_b]\{\dot{y}_b\} + [K_b]\{y_b\} \\ &\quad = [K_{b-v}]\{y_v\} - [K_{b-vb}]\{y_b\} + \{F_{b-r}\} + [C_{b-v}]\{\dot{y}_v\} \\ &\quad - [K_{b-cb}]\{y_b\} - [C_{b-b}]\{\dot{y}_b\} + \{F_{b-cr}\}. \end{aligned} \tag{35}$$

Equations (34) and (35) can be combined and rewritten in a matrix form as:

$$\begin{bmatrix} M_b & \\ & M_v^N \end{bmatrix} \begin{Bmatrix} \ddot{y}_b \\ \ddot{y}_v \end{Bmatrix} + \begin{bmatrix} C_b + C_{b-b} & -C_{b-v} \\ -C_{v-b} & C_v^N + C_{v-v}^N \end{bmatrix} \begin{Bmatrix} \dot{y}_b \\ \dot{y}_v \end{Bmatrix} + \begin{bmatrix} K_b + K_{b-vb} + K_{b-cb} & -K_{b-v} \\ -K_{v-b} - K_{v-cb} & K_v^N + K_{v-v}^N \end{bmatrix} \begin{Bmatrix} y_b \\ y_v \end{Bmatrix} = \begin{Bmatrix} F_{b-r} + F_{b-cr} \\ -F_{v-r} - F_{v-cr} + F_G^N \end{Bmatrix}, \tag{36}$$

where C_{b-b}, C_{b-v}, C_{v-b}, K_{b-vb}, K_{b-cb}, K_{b-v}, K_{v-b}, K_{v-cb}, F_{b-r}, F_{b-cr}, F_{v-r}, and F_{v-cr} are resulted due to the coupling effect between the bridge and vehicles. When a vehicle travels on the bridge, the position of the patch contact changes with time, which means the road roughness $r(x)$ at the patch contact and the relationship function $[N_b]$ are both time-dependent terms, indicating that all the additional terms in Eq. (36) are time-dependent terms. Eq. (36) can be solved by the *Newmark*β-method in the time domain.

2.4. *Road surface condition*

The road surface condition is an important factor that affects the dynamic responses of both the bridge and vehicles. A road surface profile is usually assumed to be a zero-mean stationary Gaussian random process and can be generated through an inverse Fourier transformation based on a power spectral density (PSD) function[25] as:

$$r(x) = \sum_{k=1}^{N} \sqrt{2\varphi(n_k)\Delta n}\ \cos(2\pi n_k x + \theta_k), \tag{37}$$

where θ_k is the random phase angle uniformly distributed from 0 to 2π; $\varphi(\bullet)$ is the PSD function (m^3/cycle) for the road surface elevation; and n_k is the wave number (cycle/m). In the present study, the following PSD function[2] has been used:

$$\varphi(n) = \varphi(n_0)\left(\frac{n}{n_0}\right)^{-2} \quad (n_1 < n < n_2), \tag{38}$$

where n is the spatial frequency (cycle/m); n_0 is the discontinuity frequency of $1/2\pi$ (cycle/m); $\varphi(n_0)$ is the roughness coefficient (m^3/cycle) whose value is chosen depending on the road condition; and n_1 and n_2 are the lower and upper cut-off frequencies, respectively. The International Organization for Standardization (ISO)[26] has proposed a road roughness classification index from A (very good) to H (very poor) according to different values of $\varphi(n_0)$. In this paper, the classification of road roughness based on the Ref. 26 is used.

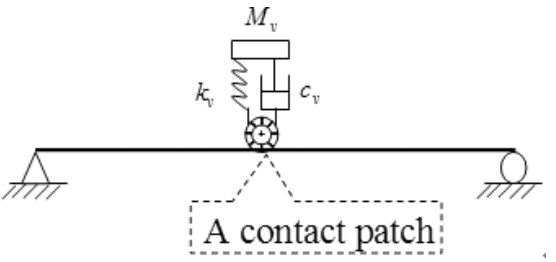

Fig. 4. A simply-supported beam subjected to a moving sprung mass system.

3. Numerical Simulations and Verification

In order to study the effect of the patch contact on the bridge vibration and to verify the present method of the bridge-vehicle system, a typical bridge-vehicle model shown in Fig. 4 was studied.

Figure 4 shows a simply-supported beam subjected to a moving sprung mass system, which is similar to the model studied by Yang *et al.*[7] The only difference is that in Yang's study, the contact condition of the tire and road surface was considered as a point contact, rather than a patch contact. The vehicle sprung mass M_v is supported by a dashpot-spring unit with the spring constant k_v and damping c_v. For illustration, the effect of the tire mass will be neglected. The beam parameters are: Young's modules $E = 2.87\,\text{GPa}$, moment of inertia $I = 2.90\,\text{m}^4$, per-unit-length mass $\text{m} = 2303\,\text{kg/m}$, and beam length $L = 25\,\text{m}$.

3.1. *Effect of patch contact*

According to Elseifi *et al.*[27] study on the patch contact, the length of tire patch contact mainly depends on the vehicular load and the tire type, and is geometrically related with the deformation Δ. Therefore, effect of the tire patch contact on the mid-span displacement of the bridge can reflect the effect of the deformation Δ. Theoretically speaking, both values are time-dependent variables since the tire reaction is variable due to the dynamic effects. However, both values are assumed as constants here based on the static tire reactions. Tire stiffness and damping can be assumed as $k_{ty} = 44456\,\text{N/m}$ and $c_{ty} = 1100\,\text{N.s/m}$, respectively, and the dimension of this patch contact can be simulated as a rectangle with a size of $116\,\text{mm} \times 235\,\text{mm}$, where 116 mm is the length and 235 mm is the width of the patch. In order to study the effect of the patch contact lengths on the mid-span displacement of the bridge, three different lengths for the patch contact are studied, namely, $l_{ty} = 0\,\text{mm}$, $l_{ty} = 116\,\text{mm}$, and $l_{ty} = 2 \times 116\,\text{mm}$.

The mid-span displacements of the beam were studied by Yang *et al.*[7] for the sprung mass with a speed $v = 100\,\text{km/h}$. Therefore, the same speed was also used for comparison and the effect of the patch contact lengths on the mid-span displacements of the beam were plotted in Fig. 5. As can be seen, if the length of the patch contact $l_{ty} = 0\,\text{mm}$ (equivalent to point contact), the responses obtained by the

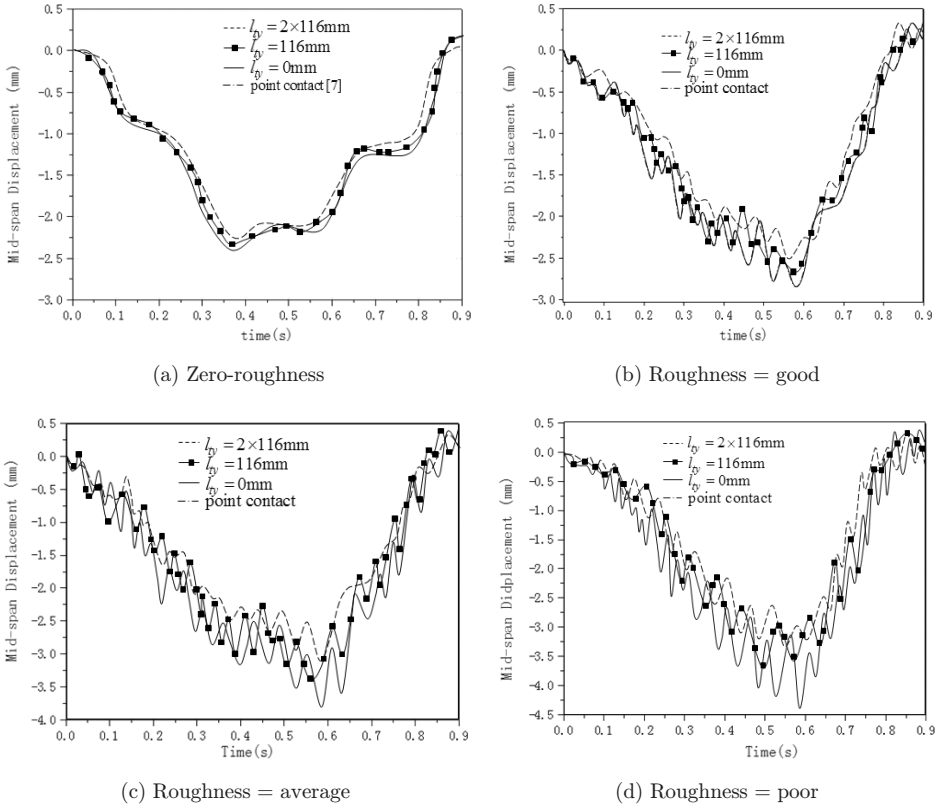

(a) Zero-roughness

(b) Roughness = good

(c) Roughness = average

(d) Roughness = poor

Fig. 5. Mid-span displacement of simply-supported beam.

present model are identical to the solutions obtained by Yang *et al.*[7] labeled as point contact in Fig. 5. By comparing Figs. 5(a) to 5(d), one observes that, if the road surface classification is zero-roughness, the difference of the effects of the patch contact and point contact on the mid-span deflections is very small, and thus the patch contact can be simplified as the point contact. However, when the road surface classification ranges from the Good to Poor, the patch contact can observably predict less deflection of the bridge than that of the point contact, and their difference increases as the road roughness classification increases. Therefore, by treating the contact condition between the tire and road surface as a point contact, one may overestimate the dynamic deflection of the bridge, especially when the road surface is rough. This may be one of the reasons why theoretical simulations usually overestimate the dynamic effects of field tests. However, the assumption of the contact condition between the tire and road surface as a point contact results in a conservative design.

3.2. *Effect of tire stiffness and damping*

The effects of stiffness and damping of vehicle suspensions on the bridge response have been studied by many researchers.[7,13,28] However, few studies on the effects of the tire stiffness and damping on the bridge response were reported, especially for the patch contact condition.

To study the effect of tire stiffness on the bridge response, three values of tire stiffness $0.2\,k_{ty}$, k_{ty}, and $2\,k_{ty}$ are considered. The contact between the tire and road surface is assumed to be a patch contact. The mid-span displacements of the beam are plotted in Fig. 6. As it can be seen from the figure, the displacements increase with the increase of the tire stiffness; the degree of the stiffness effect increases with the increase of the road roughness classification. As the tire stiffness increases from $0.2k_{ty}$ to $2k_{ty}$, and the road roughness classification increases from zero-roughness to Poor, the mid-span displacements increase from 2.9% to 12.67%.

Three values of the tire damping are considered, that is, $0.2c_{ty}$, c_{ty}, and $2c_{ty}$. The mid-span displacements of the beam are plotted in Fig. 7 using a patch contact condition. As it can be seen from the figure, the displacements decrease as the tire

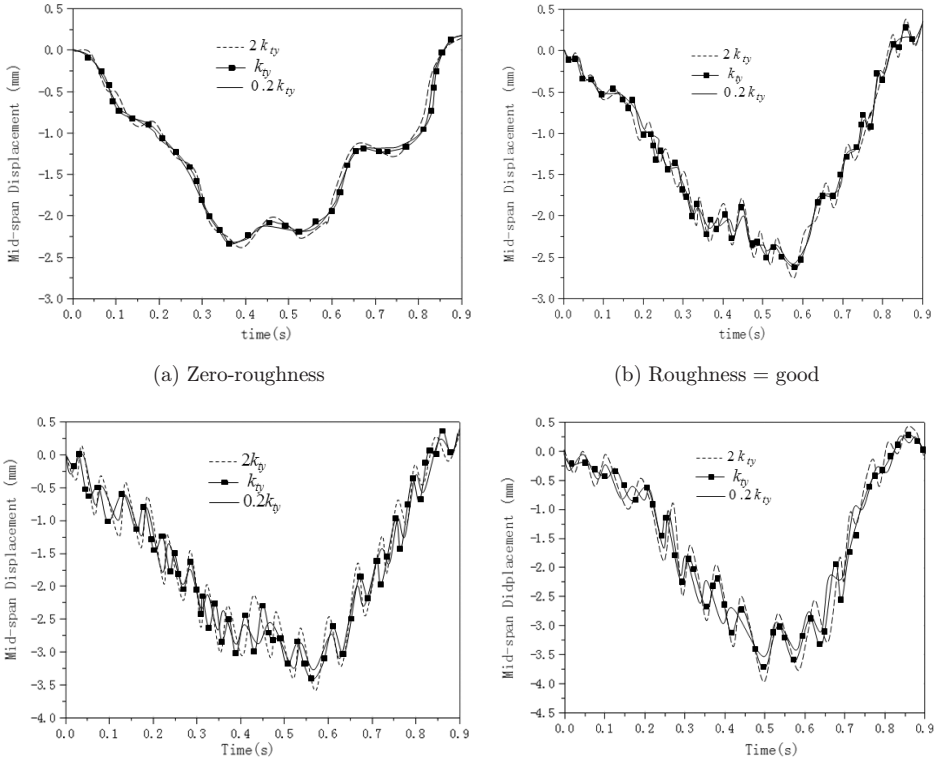

(a) Zero-roughness

(b) Roughness = good

(c) Roughness = average

(d) Roughness = poor

Fig. 6. Effect of tire stiffness.

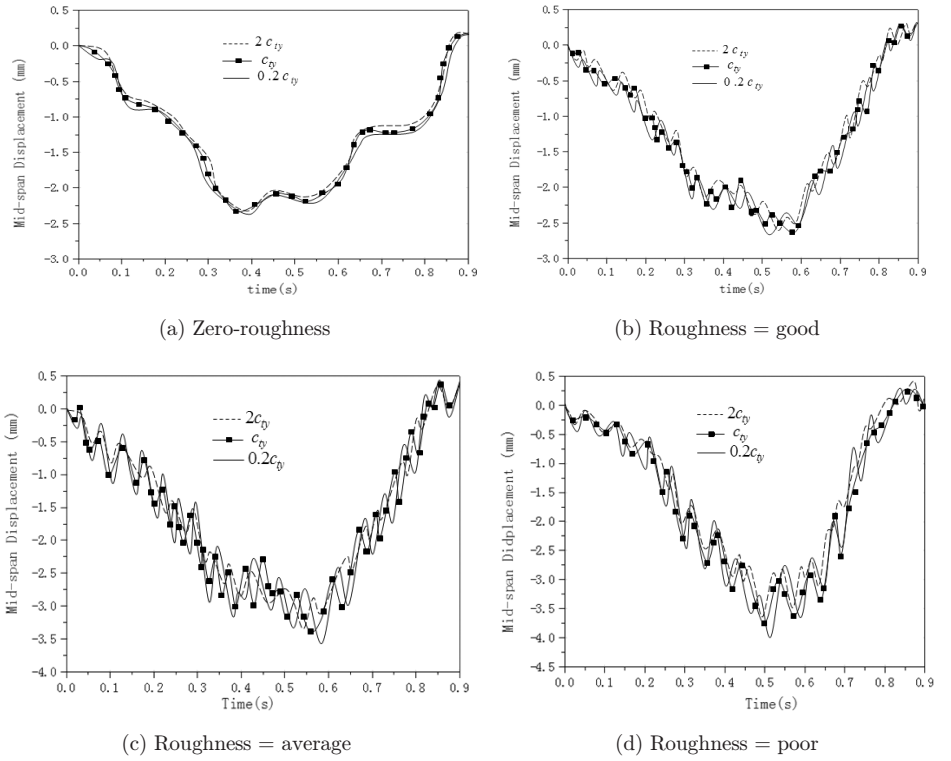

(a) Zero-roughness

(b) Roughness = good

(c) Roughness = average

(d) Roughness = poor

Fig. 7. Effect of tire damping.

damping increases; the degree of the damping effect increases with the increase of the road roughness classification. As the tire damping increases from $0.2c_{ty}$ to $2c_{ty}$, and the road roughness classification increases from zero-roughness to Poor, the mid-span displacements decrease from 3.11% to 11.16%.

4. Field Test Studies

To verify the accuracy and efficiency of the present method for studying dynamic response of the bridge-vehicle system, field verifications are necessary. Field tests were conducted on the Luping Bridge located at Luping Town in Hunan Province, China. The bridge is a seven-span straight continuous beam bridge, each span measuring 40 m in length with zero skew angles. The deck consists of 5 longitudinal T-beams and 28 transverse beams. Dynamic field tests were performed on the bridge, and the mid-span deflection of the fourth span from Luping town to Huaihua town direction was recorded on the surface of the Girder 3 (shown Fig. 8). Modal analysis was performed using the ambient vibration method. The details of measuring the bridge displacements and modal test are not given here due to the page limitation. The first three natural frequencies of the vertical bending modes of the deck were

(a) The side view of Luping bridge

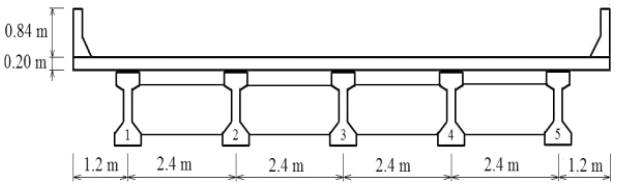

(b) Cross section of Luping bridge

Fig. 8. Luping bridge.

obtained. Figure 8 shows the side view of the bridge and the cross section of Luping bridge, and Fig. 9 shows the solid elements of the ANSYS program.

4.1. *Bridge model updating*

Model updating technique is one of the very important steps in obtaining an accurate FE model, which can predict more closely the performance of a real bridge. The techniques have moved away from direct approaches that reproduce the measured modal data, to methods based on optimization that allows a range of measurements and physical parameters to be used.[29,30]

In the present finite element model, the bridge deck, girders, diaphragms, shoulder, and the railing are all modeled using the solid elements, which have three translational DOFs for each node. The rubber bearings are modeled using equivalent beam elements with six DOFs for each node, and rigid connections are assumed between girders and diaphragms, and between girders and bridge deck. Because of their uncertainties, five parameters are selected as variables, then they are updated using the genetic algorithm (GA) by minimizing an objective function built up using the residuals between the measured bridge responses and predicted responses from the expressed relationships.[31] The five main parameters are the Young's modulus of the concrete of the girders and piers, the density of the concrete of the girders and piers, and the Young's modulus of the rubber bearings, represented by X1, X2, X3, X4, and X5 in Table 1, respectively. Both the updated results for the five parameters and their differences from the original values are shown in Table 1. As it can be seen from Table 1, both the Young's modules of the concrete of the girders and piers have

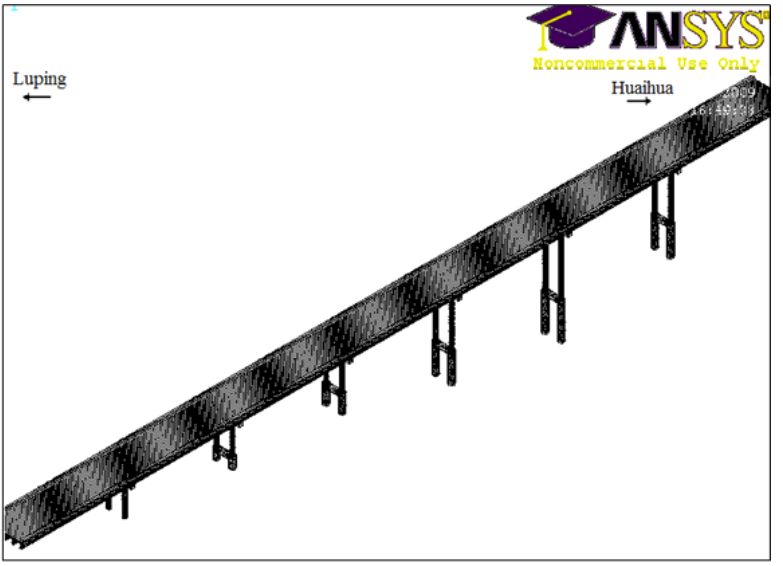

Fig. 9. FE model of Luping bridge.

Table 1. Updated results for the five parameters.

Parameter	X1(GPa)	X2(GPa)	X3(kg/m^3)	X4(kg/m^3)	X5(MPa)
Original	32.5	34.5	2500	2500	200
Updated	36.8	40.4	2298	2408	157
Difference (%)	13.23	17.10	−8.08	−3.68	−21.5

increased whereas the mass density of concrete of both the girders and piers have decreased. Many factors such as the water cement ratio of concrete mix may cause the variation of the mass density of concrete. The decrease of the Young's modulus of the rubber bearings could be due to the uncertain restraint condition of the bearing at the supports. We cannot also exclude the possibility that the changes of parameters are numerical rather than physical, a common issue in model updating. The natural frequencies were determined by observing the peaks of the average normalized power spectral densities as shown in Fig. 10. The reconstructed first three natural frequencies of the vertical bending modes of the deck, predicted using the updated finite element model, and their small differences between the measured ones are shown in Table 2.

4.2. *Road surface condition*

The road surface condition is an important factor that affects the dynamic responses of both the bridge and vehicles.[25,32] In order to examine the effect of road roughness on the accuracy of the present method, the road roughness of the bridge was measured before the dynamic test. Also, the vertical road roughness of the left and

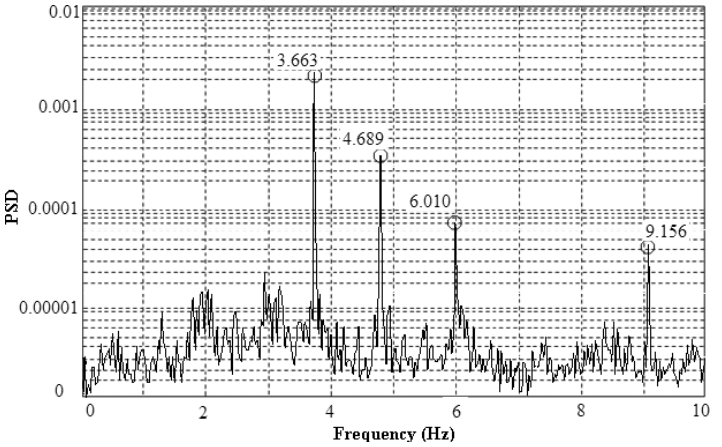

Fig. 10. Average normalized power spectral density of the ambient measurements.

Table 2. The reconstructed first three natural frequencies of vertical bending modes.

Natural frequencies (Hz)	First	Second	Third
Measured	3.663	4.689	6.010
Reconstructed	3.646	4.775	6.162
Difference (%)	−0.464	1.834	2.527

right contact patches, corresponding to the vehicular left and right tires acting on the road surface, were measured. The bump-caused dynamic problem, induced by the faulting between the approach slab and the bridge deck, was studied. The bumps were simulated using two wood planks (named Bump-I and Bump-II) with a height of 0.025 m and 0.050 m, respectively. Figure 11 shows the road roughness of the bridge used in this study.

4.3. *The test vehicle parameters*

The mechanical and geometric properties of the test truck are listed in Table 3. Only the dimensions, axle loads, and total weight of the vehicle were actually measured and can then be treated as reliable information. The other information including stiffness, damping, etc. is not available and is assumed to be the same as that obtained from Shi.[13]

4.4. *Comparison of numerical simulations and measurements*

4.4.1. *Effect of different vehicle speeds*

To account for the effects of vehicles traveling at different speeds, four levels of vehicle speeds have been used: 20 km/h, 40 km/h, 60 km/h, and 80 km/h. In all four cases, the vehicle is traveling along the central line of the bridge with a constant

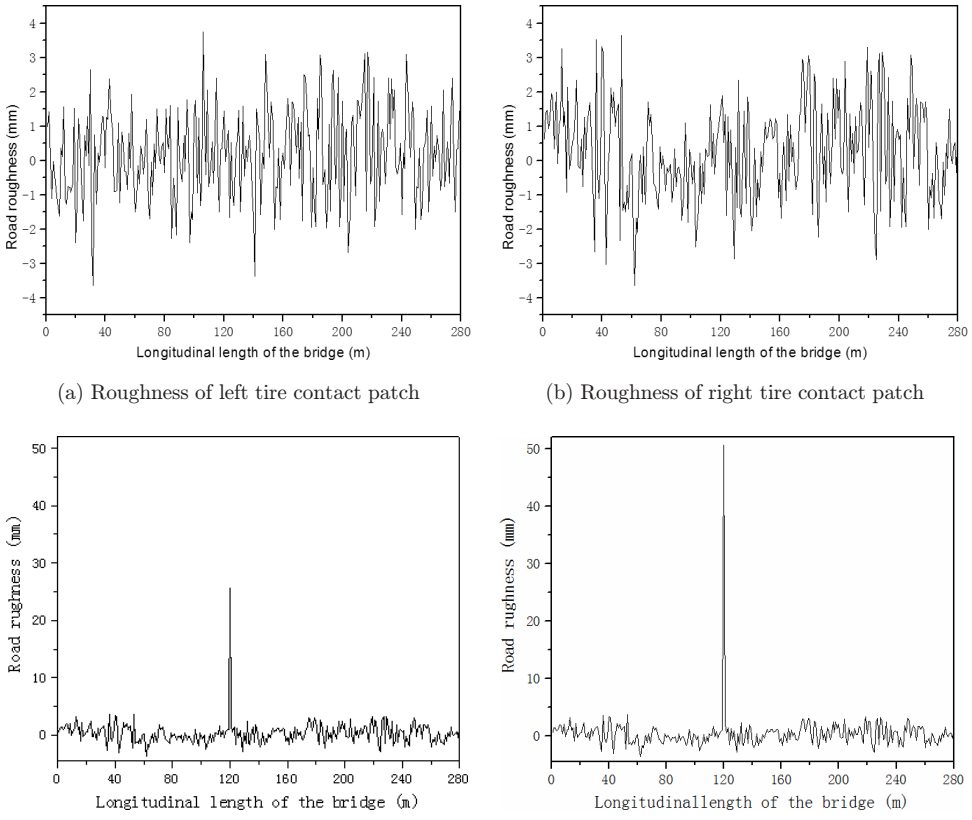

(a) Roughness of left tire contact patch

(b) Roughness of right tire contact patch

(c) Roughness with wood bump (Bump-1)

(d) Roughness with wood bump (Bump-2)

Fig. 11. Road roughness of the bridge.

speed. Figure 12 shows the comparison of the simulations and measurements of the mid-span displacements. It can be seen that the general trend of the simulated and measured mid-span displacements of the beam matches very well, though some values at the same time (t) are different between the simulated and measured values; the simulations using the patch contact matches much better than that using the point contact. The difference between the simulations and measurements can be explained by two reasons. Firstly, the bridge model and the vehicle model may be understandably different from the real bridge and truck used in the test. Secondly, the environment (such as temperature and wind) would affect the accuracy of the measuring instruments, along with the human errors in controlling the truck locations.

4.4.2. *Effect of number of vehicles*

Usually, more than one vehicle is traveling on a bridge at the same time. To verify the proposed method for this situation, two case studies were carried out with the

Table 3. Truck parameters.

Mass of truck body m_t	28 054 kg
Pitching moment of inertia of truck body I_{zt}	172,160 kg.m^2
Rolling moment of inertia of truck body I_{xt}	61,496 kg.m^2
Mass of truck front axle m_{a1}	1415 kg
Rolling moment of inertia of front axle I_{xa1}	2260 kg.m^2
Mass of truck rear axle m_{a2}	2834 kg
Rolling moment of inertia of rear axle I_{xa2}	2260 kg.m^2
Suspension spring stiffness of the first axle K^1_{sy}, K^2_{sy}	242604 (N/m)
Suspension damper coefficient of the first axle D^1_{sy}, D^2_{sy}	2190 (N.s/m)
Suspension spring stiffness of the second axle K^3_{sy}, K^4_{sy}	1903172 (N/m)
Suspension damper coefficient of the second axle D^3_{sy}, D^4_{sy}	7882 (N.s/m)
Radial direction spring stiffness of the tire k_{ty}	266670 (N/m)
Radial direction spring damper coefficient of the tire c_{ty}	1900 (N.s/m)
Length of the patch contact	350 mm
Width of the patch contact	250 mm
Distance between the front and rear axles l_1	4.85 m
Distance between the front and the center of the truck l_2	3.73 m
Distance between the rear axle and the center of the truck l_3	1.12 m
Distance between the right and left axles s_1, s_2	2.40 m

vehicle moving at 40 km/h. In the first case, the two vehicles travel along the same route, with one traveling in front of the other at a distance of 10 m. In the second case, the two vehicles travel along two different routes, with one traveling in front of the other at a distance of 10 m in the longitudinal direction. Figure 13 shows the comparison of the simulated solutions and measurements. It can be seen that the trend of the mid-span displacement of the simulated solutions and measurements matches very well.

4.4.3. *Effect of faulting condition*

To study the bump-caused dynamic problem, induced by the faulting between the approach slab and the bridge deck, a wood bump (Bump-I or Bump-II) was placed at the end of the third span to simulate the faulting condition, with the vehicle moving at 40 km/h. The time history of the mid-span deflection of the test span under the wood bump is presented in Fig. 14. It is clear in the figure that the simulations using the patch contact and the measurements match much better than that using the point contact, especially for the maximum deflection.

5. Conclusion

Presented herein is a new method that considers the effect of the patch contact on the dynamic response of the bridge-vehicle coupling system. The vehicle tire of the new model was modeled as a two-dimensional elementary spring model, and the patch contact of the tire and road surface was assumed as a rectangle. The bridge-vehicle coupling equations were established by combining the equations of motion of both

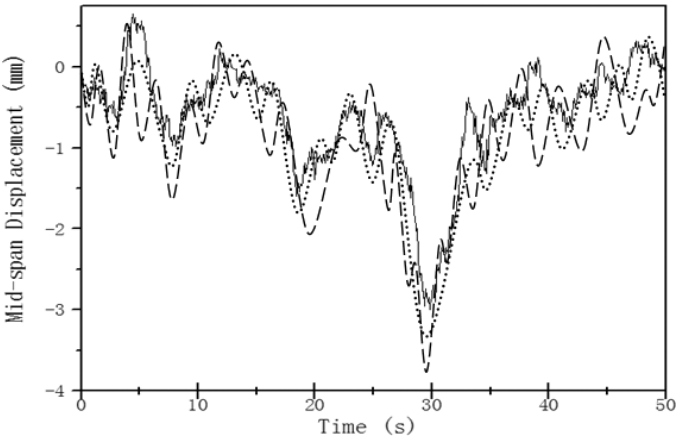

(a) Vehicle speed = 20 km/h

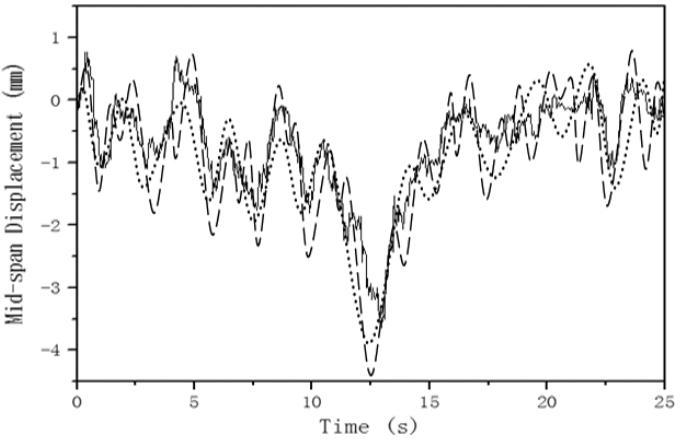

(b) Vehicle speed = 40 km/h

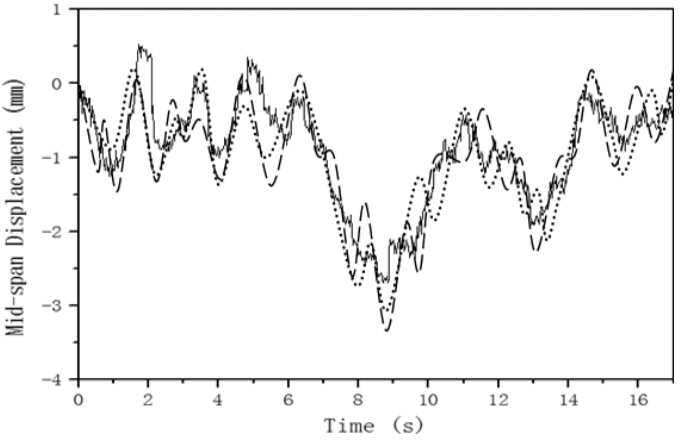

(c) Vehicle speed = 60 km/h

Fig. 12. Comparison of simulated and measured solutions of mid-span displacement (—— measured; ------, patch contact; — —, point contact).

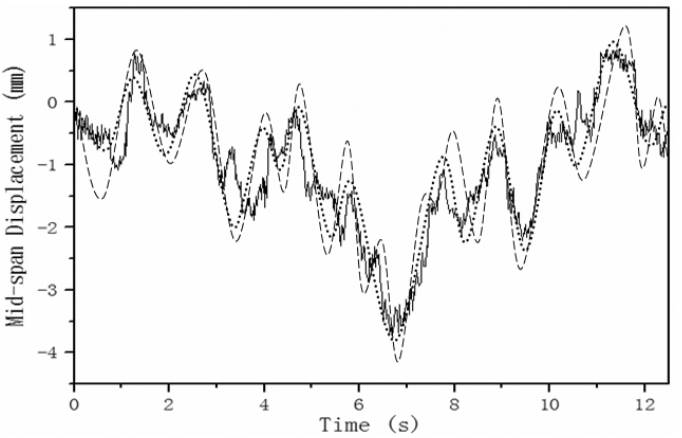

(d) Vehicle speed = 80 km/h

Fig. 12. (*Continued*)

the bridge and vehicle using the displacement relationship and the interaction force relationship at the patch contact. A series of simulation studies were carried out in which the effects of various factors such as vehicle speed, tire stiffness and damping, size of the patch contact, number of vehicles, and faulting condition were investigated to demonstrate the methodology. The results show that:

(1) If the road surface classification is zero-roughness, the patch contact can be simplified as the point contact;
(2) If the road surface classification ranges from the Good to Poor, the difference of the effect of the patch contact and point contact on the mid-span deflections increases as the road roughness classification increases. By treating the contact condition between the tire and road surface as a point contact, one may overestimate the dynamic deflection of the bridge. However, by assuming the contact condition between the tire and road surface as a point contact, the design is conservative.
(3) Increasing the tire stiffness or decreasing the tire damping increases the response of the bridge, and the degree of the influence increases as the road roughness classification increases;
(4) Comparison with the measurement shows that the simulated solution considering the patch contact matches much better than that by assuming the point contact. This is especially true when studying the faulting condition effect where the simulation using the point contact may result in significant errors. However, it should be noted that some parameters of the test truck are not available and are based on assumed values. Thus, the reader should be cautious about this conclusion;

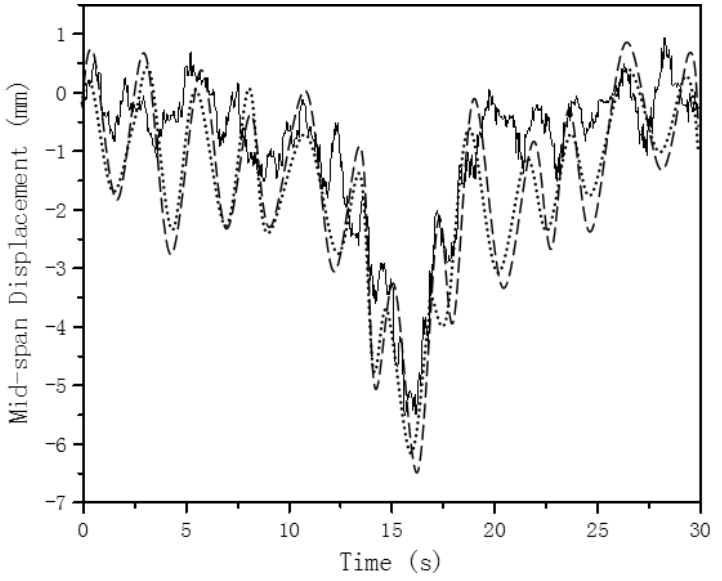

(a) First case

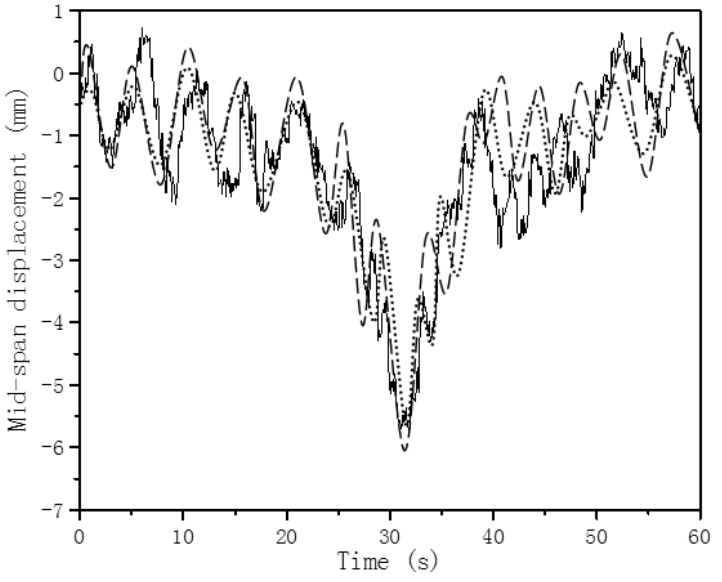

(b) Second case

Fig. 13. Comparison of simulated and measured solutions for two vehicles (—— measured; ------, patch contact; — —, point contact).

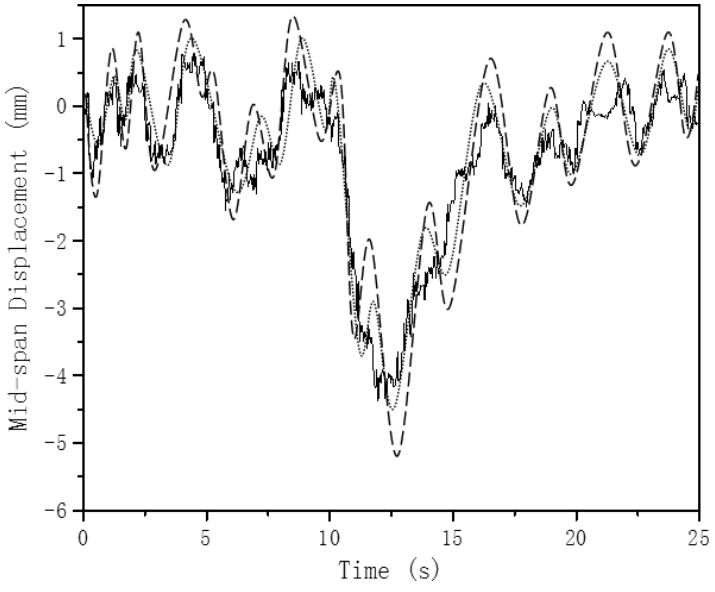

(a) Bump-I

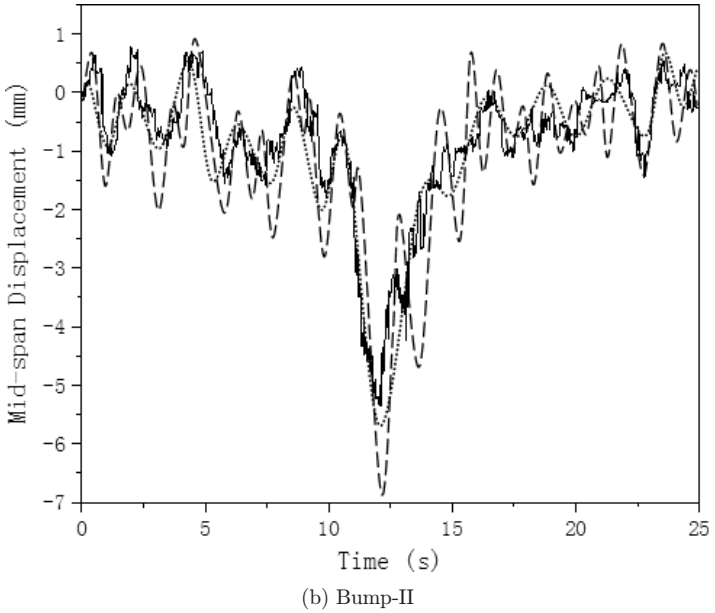

(b) Bump-II

Fig. 14. Comparison of simulated and measured solutions for wood bump effect (—— measured; ------, patch contact; — —, point contact).

(5) Comparison of theoretical simulations and field measurements shows that the proposed method can be applied to study the interaction of bridge-vehicle coupling system with good accuracy.

Acknowledgment

The first author appreciates the financial support from the Ministry of Education of the People's Republic of China. This scholarship makes his visit to Louisiana State University possible. The opinions and statements do not necessarily represent those of the sponsor.

References

1. L. Fryba, Response of a beam to a rolling mass in the presence of adhesion, *Acta Technica CSAV* **19**(6) (1974) 673–687.
2. T. L. Wang, D. Z. Huang and M. Shahawy, Dynamic response of multi-girder bridges, *Journal of Structural Engineering* **118**(8) (1992) 2222–2238.
3. M. F. Green and D. Cebon, Dynamic interaction between heavy vehicles and highway bridges, *Computers and Structures* **62**(2) (1997) 253–264.
4. S. R. Chen and C. S. Cai, Accident assessment of vehicles on long-span bridges in windy environments, *Journal of Wind Engineering and Industrial Aerodynamics* **92** (2004) 991–1024.
5. S. S. Law and X. Q. Zhu, Bridge dynamic responses due to road surface roughness and braking of vehicle, *Journal of Sound Vibration* **282**(5) (2005) 805–830.
6. Y. Zhang, C. S. Cai and X. M. Shi, Vehicle induced dynamic performance of a FRP versus concrete slab bridge, *ASCE Journal of Bridge Engineering* **11**(4) (2006) 410–419.
7. Y. B. Yang, J. D. Yau and Y. S. Wu, *Vehicle-Bridge Interaction Dynamics with Applications to High-Speed Railways* [M]. World Scientific Publishing Co. Pte. Ltd, (2004).
8. X. Q. Zhu and S. S. Law, Dynamic axle and wheel loads identification: Laboratory studies, *Journal of Sound and Vibration* **268**(5) (2003) 855–879.
9. S. S. Law, J. Q. Bu and X. Q. Zhu, Vehicle axle loads identification using finite element method, *Journal of Engineering Structures* **26**(8) (2004) 1143–1153.
10. T. L. Wang, M. Shahawy and D. Z. Huang, Impact in highway prestressed concrete bridges, *Computer and Structures* **44**(3) (1992) 525–534.
11. J. S. Lee and J. K. Hammond, Estimation of parameters of a non-stationary random process due to a moving source based on the covariance-equivalent model, *Mechanical Systems & Signal Processing* **9**(5) (1995) 509–514.
12. T. L. Wang and C. H. Liu, *Influence of Heavy Trucks on Highway Bridges*. Rep. No. FL/ DOT/RMC/ 6672-379, Florida Department of Transportation, Tallahassee, FL (2000).
13. X. M. Shi, *Structural Performance of Approach Slab and its Effect on Vehicle Induced Bridge Dynamic Response*. PhD Dissertation, Louisiana State University, Baton Rouge, LA (2006).
14. T. Pinkaew and P. Asnachinda, Experimental study on the identification of dynamic axle loads of moving vehicles from the bending moments of bridges, *Engineering Structures* **29**(9) (2007) 2282–2293.
15. V. K. Garg and R. V. Dukkipati, *Dynamics of Railway Vehicle Systems.* Academic Press, Canada (1984).
16. Y. B. Yang and B. H. Lin, Vehicle-bridge interaction analysis by dynamic condensation method, *Journal of Structural Engineering* **121**(11) (1995) 1636–1643.

17. Y. B. Yang and J. D. Yau, Vehicle-bridge interaction element for dynamic analysis, *Journal of Structural Engineering* **123**(11) (1997) 1512−1518.
18. B. Yang, C. A. Tan and L. A. Bergman, Direct numerical procedure for solution of moving oscillator problems, *Journal of Engineering Mechanics* **126**(5) (2000) 462−469.
19. G. Gim and P. E. Nikravesh, Analytical model of pneumatic types for vehicle dynamic simulations Part 1. Pure slips, *International Journal of Vehicle Design* **11**(5) (1990) 589−618.
20. G. Gim and P. E. Nikravesh, Analytical model of pneumatic types for vehicle dynamic simulations Part 2. Comprehensive slips, *International Journal of Vehicle Design* **12**(1) (1991) 19−39.
21. G. Gim and P. E. Nikravesh, Analytical model of pneumatic types for vehicle dynamic simulations Part 3. Validation against experimental data, *International Journal of Vehicle Design* **12**(2) (1991) 217−228.
22. B. G. Kao, A three-dimensional dynamic tire model for vehicle dynamic simulations, *Tire Science and Technology* **28**(2) (2000) 72−95.
23. X. Q. Yan, Y. S. Wang and X. J. Feng, Study for the endurance of radial truck tires with finite element modeling, *Mathematics and Computers in Simulation* **59** (2002) 471−488.
24. L. Yu and T. H. Chan, Recent research on identification of moving loads on bridges, *Journal of Sound and Vibration* **305**(1−2) (2007) 3−21.
25. C. J. Dodds and J. D. Robson, The description of road surface roughness, *Journal of Sound and Vibration* **31**(2) (1973) 175−183.
26. International Organization for Standardization (ISO). *Mechanical Vibration-Road Surface Profiles-Reporting of Measured Data*. ISO 8068: (E), ISO, Geneva (1995).
27. M. Elseifi, I. L. Al-Qadi and P. J. Yoo, *Pavement Damage due to Different Tires and Vehicle Configurations*, Report submitted to Michelin Americas Research and Development Corporation. The roadway infrastructure group Virginia Tech Transportation Institute 3500 transportation research plaza, Blacksburg, VA 2460 (2004).
28. H. Y. Li J. Wekezer and L. Kwasniewsk, Dynamic response of a highway bridge subjected to moving vehicles, *Journal of Bridge Engineering* **13**(5) (2008) 439−448.
29. J. L. Zapico, M. P. Gonzalez and M. I. Friswell, Finite element model updating of a small scale bridge, *Journal of Sound and Vibration* **268**(5) (2003) 993−1012.
30. T. Pinkaew, Identification of vehicle axle loads from bridge responses using updated static component techniques, *Engineering Structures* **28**(11) (2006) 1599−1608.
31. L. Deng and C. S. Cai, Bridge model updating using response surface method and genetic algorithm, *Journal of Bridge Engineering* (2009) (Accepted).
32. K. Chompooming and M. Yener, The influence of roadway surface irregularities and vehicle deceleration on bridge dynamics using the method of lines. *Journal of Sound Vibration* **183**(4) (1995) 567−589.